

FABRICATION AND CHARACTERIZATION OF POROUS III-NITRIDES ALLOYS FOR APPLICATION IN HYDROGEN GAS SENSING DEVICES

by

ROSFARIZA BINTI RADZALI

**Thesis submitted in fulfillment of the requirements
for the degree of
Doctor of Philosophy**

May 2017

ACKNOWLEDGEMENT

Alhamdulillah, all praises to Allah, unto Him belongs all knowledge and understanding.

First and foremost I would like to acknowledge and extend my deepest gratitude to my main supervisor, Prof. Dr. Zainuriah Hassan who was very helpful and offered invaluable advice and support. I am deeply indebted to her for guiding me through the tough times and always being positive about my work. I also would like to express my deepest appreciation to my co-supervisors, Dr. Yam Fong Kwong and Dr. Norzaini Zainal, for their advice, knowledge, and support. I am very honored and blessed to have had the opportunity to work with kind and supportive supervisors.

I would also like to express my appreciation to the staff in the Institute of Nano Optoelectronics Research and Technology (INOR) USM, especially Mr. Anas, Madam Bee Choo, Mr. Yushamdan, and Mr. Jamil for their co-operation and technical assistance. Many thanks to my beloved colleagues - Ezzah, Waheeda, Azharul, Ikram, Esmad, Alvin, Chin and Ainor for their relentless help, ideas and technical contributions.

I would also like to convey thanks to UiTM for awarding me the scholarship that allowed me to conduct this study. Finally, I wish to express my love and gratitude to my husband, Shahrul and my mother, Pn. Fatimah for their support, understanding, patience, and encouragement throughout the tough journey of my PhD study. Thank you for taking care of the children while I was busy with my study. To my children - Danish, Irfan, Nafiz and the new baby, mama loves all you with all my heart. Without the support from my family, I would not have been able to complete my study. Thank you all so much and Terima Kasih.

TABLE OF CONTENTS

ACKNOWLEDGEMENT	ii
TABLE OF CONTENTS	iii
LIST OF TABLES	viii
LIST OF FIGURES	ix
LIST OF SYMBOLS	xv
LIST OF MAJOR ABBREVIATIONS	xviii
ABSTRAK	xx
ABSTRACT	xxii
CHAPTER 1 INTRODUCTION	1
1.1 Introduction to III-Nitrides	1
1.2 Research Problem and Motivation	2
1.3 Research Objectives	4
1.4 Originality of the Research Work	5
1.5 Limitation of Study	6
1.6 Outline of the Thesis	6
CHAPTER 2 LITERATURE REVIEW	8
2.1 Introduction	8
2.2 Overview of Porous Semiconductors	8
2.3 Overview of Porous III-nitrides	12
2.4 Overview of the Process of Fabricating Porous III-nitrides	14
2.4.1 Fabrication of Porous III-nitrides by Bottom-up Technique	15
2.4.2 Fabrication of Porous III-nitrides by Dry Etching Technique	15
2.4.3 Fabrication of Porous III-nitrides by Wet Etching Technique	16
2.4.3(a) Metal-assisted Electroless Etching	16

2.4.3(b) Photoelectrochemical (PEC) Etching	18
2.5 Overview of Hydrogen Gas Sensors	23
2.5.1 III-nitrides Hydrogen Gas Sensors	23
2.5.2 Porous III-nitrides Based Hydrogen Gas Sensors	24
2.6 Summary	26
CHAPTER 3 THEORY	27
3.1 Introduction	27
3.2 Photoelectrochemical (PEC) Etching	27
3.2.1 Photoelectrochemical (PEC) Etching Mechanism of III-nitrides	27
3.3 Metal-Semiconductor Contact	30
3.3.1 Schottky Contact and Barrier Height	31
3.4 Hydrogen Gas Sensor	33
3.4.1 Gas Sensing Mechanism	34
3.4.2 Sensitivity	36
3.4.3 Response and Recovery Times	36
CHAPTER 4 METHODOLOGY	38
4.1 Introduction	38
4.2 Growth of III-nitrides Layer by Plasma-Assisted Molecular Beam Epitaxy (PA-MBE)	40
4.2.1 GaN Films Grown by PA-MBE	40
4.2.2 InGaN Films Grown by PA-MBE	41
4.2.3 Commercial Samples of InAlGa _N Films Grown by PA-MBE	42
4.3 Porous III-Nitrides Etching	43
4.4 Fabrication and Characterization of Gas Sensor	45
4.4.1 Fabrication of Hydrogen Gas Sensor	46

4.4.2	Experimental Setup and Characterization of Gas Sensor	47
4.5	Characterization Measurements	48
4.5.1	Field Emission-Scanning Electron Microscopy (FE-SEM) and Energy Dispersive X-ray Spectrometer (EDX)	49
4.5.2	Image Processing	50
4.5.3	Atomic Force Microscopy (AFM)	51
4.5.4	High Resolution X-Ray Diffraction (HR-XRD)	52
4.5.5	Photoluminescence (PL) and Raman Scattering	55
4.5.6	Summary	56
CHAPTER 5 FABRICATION OF POROUS GaN FOR HYDROGEN GAS		
	SENSOR	58
5.1	Introduction	58
5.2	Fabrication of Porous GaN under Different Etching Durations	59
5.2.1	FE-SEM Analysis	59
5.2.2	AFM Analysis	61
5.2.3	HR-XRD Analysis	62
5.2.4	Raman Scattering	66
5.3	Non-porous and Porous GaN Based Hydrogen Gas Sensors	67
5.4	Summary	71
CHAPTER 6 FABRICATION OF POROUS InGaN FOR HYDROGEN GAS		
	SENSOR	73
6.1	Introduction	73
6.2	Fabrication of Porous InGaN/Sapphire under Different Etching Durations	74
6.2.1	FE-SEM Analysis	74

6.2.2	AFM Analysis	77
6.2.3	HR-XRD Analysis	79
6.2.4	PL Analysis	83
6.3	Fabrication of Porous InGaN/Sapphire Using Different Light Sources	85
6.3.1	FE-SEM Analysis	86
6.3.2	AFM Analysis	90
6.3.3	HR-XRD Analysis	91
6.3.4	PL Analysis	93
6.4	Non-porous and Porous InGaN Based Hydrogen Gas Sensors	96
6.5	Summary	101
CHAPTER 7 COMPARISON OF POROUS InAlGaN ON SAPPHIRE AND		
SILICON SUBSTRATES FOR HYDROGEN GAS SENSOR		103
7.1	Introduction	103
7.2	Fabrication of Porous InAlGaN/Sapphire under Different Etching Durations	104
7.2.1	FE-SEM Analysis	104
7.2.2	AFM Analysis	107
7.2.3	HR-XRD Analysis	108
7.2.4	Raman Scattering	111
7.3	Fabrication of Porous InAlGaN/Si(111) under Different Etching Durations	114
7.3.1	FE-SEM Analysis	114
7.3.2	AFM Analysis	116
7.3.3	HR-XRD Analysis	117

7.3.4 Raman Scattering	119
7.4 Non-porous and Porous InAlGaN Hydrogen Gas Sensors	121
7.5 Summary	130
CHAPTER 8 CONCLUSION AND FUTURE WORK	133
8.1 Conclusion	133
8.2 Future Work	135
REFERENCES	
APPENDICES	
LIST OF PUBLICATIONS	

LIST OF TABLES

Table 3.1:Electrical nature of ideal metal-semiconductor contacts (adapted from (Pierret, 1996)).....	31
Table 5.1: Estimation of total pore area and porosity for porous GaN etched under different etching durations	61
Table 6.1: Summary data of estimated total pore area and porosity for porous InGaN under different etching durations	76
Table 6.2: Surface roughness in RMS value and estimated average pore depth of non-porous and etched samples fabricated using different light sources.....	91
Table 6.3: FWHM of rocking curves at (0002) and (1012) planes and estimation of dislocation density for non-porous and etched samples fabricated using different illumination of light sources.	93
Table 6.4: The SBH value of non-porous and porous InGaN gas sensors operated in ambient air and upon exposure to 0.1% H ₂ in N ₂ gas	100
Table 7.1: Summary data of estimated total pore area and porosity for porous InAlGaN/sapphire under different etching durations	106
Table 7.2: Summary data of estimated total pore area and porosity for porous InAlGaN/Si(111) under different etching durations.....	116

LIST OF FIGURES

Figure 2.1: Schematic diagram of literature review and existing research gaps.....	9
Figure 3.1: Equilibrium energy band diagram of Schottky barrier junction: (a) metal and n-type semiconductor and (b) metal and p-type semiconductor. (adapted from (Streetman and Banerjee, 2000)).....	32
Figure 3.2: Schematic band diagram and charge distribution for metal semiconductor hydrogen gas sensor at equilibrium (a) without hydrogen; and (b) with hydrogen showing the sensing mechanism in steps 1-3. (adapted from (Shao-Yen et al., 2009))	35
Figure 3.3: On-off response of a typical gas sensor	37
Figure 4.1: Flow chart of the research design in this work.....	39
Figure 4.2: Schematic diagram of the n-type GaN structure.	40
Figure 4.3: Schematic diagram of the n-type $\text{In}_{0.47}\text{Ga}_{0.53}\text{N}$ structure.	41
Figure 4.4: Schematic diagram of the unintentionally doped n-type $\text{In}_{0.10}\text{Al}_{0.10}\text{Ga}_{0.80}\text{N}$ on C-plane sapphire substrate.....	42
Figure 4.5: Schematic diagram of the unintentionally doped n-type $\text{In}_{0.10}\text{Al}_{0.10}\text{Ga}_{0.80}\text{N}$ on Si(111) substrate.	42
Figure 4.6: Schematic diagram of the experimental setup for PEC etching.....	43
Figure 4.7: HHV Auto 500 RF magnetron sputtering system: (a) photograph of the system and (b) schematic diagram.	47
Figure 4.8: The $\text{InAlGaN}/\text{Si}(111)$ porous gas sensor with Pt contacts: (a) top view image and (b) the schematic diagram.....	47
Figure 4.9: Schematic diagram of the hydrogen sensing measurement set-up system	48
Figure 4.10: Field emission-scanning electron microscopy (FE-SEM): (a) photograph of the FE-SEM system and (b) schematic diagram of FE-SEM.	49
Figure 4.11: FE-SEM images of porous InGaN sample (a) before and (b) after processing using ImageJ and the resulting output.....	51
Figure 4.12: Atomic force microscopy (AFM): (a) photograph of the system and (b) schematic diagram of basic working principle of AFM (adapted from www.circuitstoday.com)	52

Figure 4.13: High resolution XRD (PANalytical X'pert PRO MRD): (a) photo image of the system and (b) schematic diagram of the system (adapted from (Kidd, 2009))	53
Figure 4.14: Diffraction of x-rays by a crystal (adapted from (William, 1994))	53
Figure 4.15: The typical reported 2 θ -scan of HR-XRD pattern for the InGaN layer grown on sapphire substrate	55
Figure 4.16: Integrated confocal micro PL and Raman spectrometer (Jobin Yvon HR800UV): (a) photograph of the system and (b) schematic diagram of PL and Raman spectrometer system.	56
Figure 4.17: The typical reported PL spectrum of a GaN sample. The spectrum was taken from (Mohd Zaki Mohd et al., 2010)	56
Figure 5.1: Flow chart of porous GaN study	58
Figure 5.2: FE-SEM images of non-porous and porous GaN samples obtained by etching for different durations: (a) non-porous, (b) 15 minutes, (c) 30 minutes, (d) 45 minutes and (e) image with higher magnification for 45 minutes sample.	60
Figure 5.3: AFM measurements of non-porous and porous GaN samples obtained by etching for different durations: (a) non-porous, (b) 15 minutes, (c) 30 minutes and (d) 45 minutes.	62
Figure 5.4: 2 θ -scan HR-XRD patterns of non-porous and porous GaN samples.....	63
Figure 5.5: (a) Dependence of FWHM value from XRD rocking curves (RC) and (b) the dislocation density of the non-porous and porous GaN samples on different etching durations.	65
Figure 5.6: Raman spectra of the non-porous and porous GaN samples etched at different etching durations.....	66
Figure 5.7: The I-V characteristics of non-porous and porous GaN gas sensors when operated in ambient air and operated in an ambient of 0.1% H ₂ in N ₂ gas at room temperature	68
Figure 5.8: I-V characteristics: (a) non-porous GaN gas sensor and (b) porous GaN gas sensor when operated in ambient air and when operated in an ambient of 0.1% H ₂ in N ₂ gas at room temperature.	69
Figure 5.9: The on-off response of the non-porous and porous GaN gas sensors operating at room temperature and a constant voltage of 0.5 V.	70
Figure 5.10: The on-off response of the non-porous GaN gas sensor operating at room temperature and a constant voltage of 0.5 V.....	71
Figure 6.1: Flow chart of porous InGaN study	73

Figure 6.2: FE-SEM images of non-porous and porous InGaN samples obtained by etching for different durations: (a) non-porous, (b) 1 minute, (c) 10 minutes and (d) 15 minutes. Inset is the image with higher magnification.....	75
Figure 6.3: AFM measurements of non-porous and porous InGaN samples obtained by etching for different durations: (a) non-porous, (b) 1 minute, (c) 10 minutes and (d) 15 minutes.	78
Figure 6.4: Dependence of surface roughness of the samples on etching duration.	78
Figure 6.5: 2 θ -scan HR-XRD pattern of non-porous and porous InGaN samples.....	79
Figure 6.6: HR-XRD rocking curve at (a) (0002) and (b) (1012) planes of 10 minute etched porous InGaN sample.....	81
Figure 6.7: Dependence of FWHM value of RC at (0002) and (1012) planes of the non-porous and porous InGaN samples on different etching durations.....	82
Figure 6.8: Dependence of dislocation densities of the non-porous and porous InGaN samples on different etching durations.....	82
Figure 6.9: PL spectra of the non-porous and porous InGaN samples at different etching durations.	84
Figure 6.10: PL spectra of the non-porous and porous InGaN samples.....	85
Figure 6.11: FE-SEM images of non-porous and etched samples using different illumination of light sources: (a) non-porous, (b) without illumination, (c) xenon lamp and (d) mercury arc lamp (220 - 436 nm). Inset is the image with higher magnification.	88
Figure 6.12: Schematic diagram of the energy band diagram at n-InGaN/KOH electrolyte interface: (a) illumination from xenon lamp and (b) illumination from mercury arc lamp (220 - 436 nm).....	89
Figure 6.13: AFM measurements of non-porous and etched samples using different illumination of light sources: (a) non-porous, (b) without illumination, (c) xenon lamp and (d) mercury arc lamp.	90
Figure 6.14 : 2 θ -scan of HR-XRD patterns for non-porous and etched samples	92
Figure 6.15: PL spectra of the non-porous and etched samples using different light sources. Inset figure shows the PL spectra of all samples at longer wavelength.....	95
Figure 6.16: PL spectra of the non-porous and etched samples at shorter wavelength.	96

Figure 6.17: I-V characteristics of non-porous and porous InGaN gas sensors when operated in ambient air and operated in an ambient of 0.1% H ₂ in N ₂ gas at room temperature	98
Figure 6.18: The on-off response of the non-porous and porous InGaN gas sensors operating at room temperature and a constant voltage of 0.5 V.	99
Figure 7.1: Flow chart of porous InAlGaN study	103
Figure 7.2: FE-SEM images of the InAlGaN/sapphire samples etched for different etching durations: (a) non-porous, (b) 1 minute, (c) 10 minutes, (d) 15 minutes, (e) 20 minutes, (f) 30 minutes.....	106
Figure 7.3: AFM measurements of non-porous and porous InAlGaN/sapphire samples etched for different etching durations: (a) non-porous, (b) 1 minute, (c) 10 minutes, (d) 15 minutes, (e) 20 minutes, (f) 30 minutes.	107
Figure 7.4: Dependence of surface roughness of non-porous and porous InAlGaN/sapphire samples on etching duration.	108
Figure 7.5: 2 θ -scan HR-XRD patterns of non-porous and porous InAlGaN/sapphire samples.	109
Figure 7.6: FWHM of the (0002) ω -scan of non-porous and porous samples as a function of etching duration. The inset figure shows the rocking curve of the sample etched for 15 minutes.	110
Figure 7.7: Raman spectra of non-porous and porous InAlGaN/sapphire samples etched for different etching durations. The inset figure shows the Gaussian fitting for non-porous sample.....	112
Figure 7.8: Dependence of peak position of InAlGaN/sapphire E ₂ (high) mode and estimated amount of stress relaxation on etching duration.	113
Figure 7.9: FE-SEM images of the non-porous and porous InAlGaN/Si(111) samples etched for different etching durations: (a) non-porous, (b) 1 minute, (c) 5 minutes, (d) 10 minutes, (e) 15 minutes, (f) 20 minutes.....	115
Figure 7.10: AFM measurements of non-porous and porous InAlGaN/Si(111) samples etched for different etching durations.	117
Figure 7.11: 2 θ -scan HR-XRD patterns of non-porous and porous InAlGaN/Si(111) samples.....	118
Figure 7.12: InAlGaN (0002) peak of non-porous and porous samples.....	119
Figure 7.13: Raman spectra of the non-porous and porous InAlGaN/Si(111) samples etched for different etching durations; the inset shows the variation of the InAlGaN E ₂ (high) phonon mode.....	120

Figure 7.14: I-V characteristics of porous InAlGaN/Si(111) gas sensors at different etching durations: (a) 1 minute, (b) 5 minutes, (c) 10 minutes, (d) 15 minutes, (e) 20 minutes when operated in ambient air and operated in an ambient of 0.1% H ₂ in N ₂ gas at room temperature. (f) shows the I-V characteristics of the non-porous and 10 minute etched porous InAlGaN/Si(111) gas sensors.	121
Figure 7.15: Dependence of gas detection sensitivity on etching duration of non-porous and porous InAlGaN/Si(111) samples	123
Figure 7.16: Dependence of Schottky barrier heights on etching duration when sensors were operated in ambient air and with 0.1% H ₂ in N ₂ gas; the inset shows the Schottky barrier height variation ($\Delta\phi_B$) upon introduction of 0.1% H ₂ in N ₂ gas.	124
Figure 7.17: FE-SEM images of the Pt contact on the non-porous and porous InAlGaN/Si(111) samples subjected to different etching durations: (a) non-porous, (b) 1 minute, (c) 5 minutes, (d) 10 minutes, (e) 15 minutes, (f) 20 minutes	125
Figure 7.18: The on-off response of the non-porous and porous InAlGaN/Si(111) gas sensors operating at room temperature and a constant voltage of 0.5 V.....	128
Figure 7.19: Changes in the current response upon exposure to different hydrogen flow rates for (a) non-porous and (b) 10 minute etched porous InAlGaN/Si(111) gas sensors. The measurements were carried out at room temperature and a constant voltage of 0.5 V.	129

LIST OF SYMBOLS

ϵ_0	Absolute dielectric constant
T	Absolute temperature
A	Area
\AA	Armstrong
$\phi_{B(\text{air})}$	barrier height measured in ambient air
$\phi_{B(\text{H}_2)}$	barrier height measured in hydrogen gas
$\Delta\phi_B$	barrier height variation
k	Boltzmann's constant
V_{bi}	Built in voltage
b	Burger vector
e	Charge of electron
E_C	Conduction band
I	Current
I_{Air}	Current under ambient air
I_{H_2}	Current under H ₂ exposure
W	Depletion layer width
ϵ	Dielectric constant
μ	Effective dipole moment
m^*	Effective mass
χ_s	Electron affinity
q	Electron charge
m_e^*	Electron effective mass

m_o	Electron mass
ΔV	Electrostatic potential difference
E_F	Fermi energy
E_F	Fermi level of semiconductor
F	Force
β	Full wave half maximum
m_h^*	Hole effective mass
θ_i	Hydrogen atoms coverage at the interface
n	ideality factor
θ	Incident / Diffraction angle
P	Incident optical power
V_{BB}	Interfacial bend bending
d	Interplanar spacing of the crystal planes
a	Lattice constant
c	Lattice constant
ξ_m	Maximum electric field
ϕ_m	Metal work function
(hkl)	Miller indices
N_i	Number of sites per area
h	Plancks' constant
K	Proportionality factor
η	Quantum efficiency
ϵ_r	Relative dielectric constant
R_A	Resistance under ambient air
R_{h_2}	Resistance under H ₂ gas exposure

ρ	Resistivity
R	Responsivity
A^{**}	Richardson's constant
I_o	Saturation current
ϕ_B	Schottky barrier height
E_g	Semiconductor band gap
ϕ_s	Semiconductor work function
S	Sensitivity
R_s	Series resistance
σ_s	Standard deviation
ε_a	Strain along a-axis
ε_c	Strain along c-axis
σ	Stress
T	Temperature
t	Time
E_v	Valence band edge
V	Voltage
λ	Wavelength
w	Width

LIST OF MAJOR ABBREVIATIONS

a.u.	Arbitrary unit
AFM	Atomic force microscopy
CVD	Chemical Vapor Deposition
I-V	Current-Voltage
InAlGaN	Indium Aluminum Gallium Nitride
InAlGaN/Si(111)	Indium Aluminum Gallium Nitride/Silicon
InAlGaN/sapphire	Indium Aluminum Gallium Nitride/sapphire
IR	Infra-Red
eV	Electron volt
EDX	Energy Dispersive X-ray Spectrometer
FE-SEM	Field Emission-Scanning Electron Microscopy
FWHM	Full width at half maximum
HR-XRD	High Resolution X-ray diffraction
ICP	Inductively Coupled Plasma
LED	Light Emitting Diode
LO	Longitudinal Optical
MS	Metal Semiconductor
MSM	Metal Semiconductor Metal
MOCVD	Metalorganic Vapor Deposition
MBE	Molecular Beam Epitaxial
PEC	Photoelectrochemical etching
PL	Photoluminescence
RF	Radio frequency

RC	Rocking Curve
RMS	Root mean square
SEM	Scanning electron microscope
SBH	Schottky barrier height
TO	Transverse optical
UV	Ultra-Violet
XRD	X-ray diffraction

FABRIKASI DAN PENCIRIAN ALOI III-NITRIDA BERLIANG UNTUK APLIKASI PERANTI PENDERIAAN GAS HIDROGEN

ABSTRAK

Matlamat kajian yang dibentangkan adalah untuk memfabrikasikan struktur berliang III-nitrida dan menggunakannya untuk aplikasi peranti penderia gas hidrogen. Pembentukan liang pada filem-filem III-nitrida bertujuan mengurangkan ketumpatan kehelan dalam lapisan III-nitrida dan menghasilkan kawasan permukaan yang tinggi untuk aplikasi sensor gas. Dalam kajian ini, teknik punaran fotoelektrokimia (PEC) telah digunakan untuk memfabrikasi struktur GaN, InGaN dan InAlGaN berliang yang merujuk kepada sebatian III-nitrida yang terdiri daripada binari, ternari dan kuarternari, masing-masing. Sampel jenis n untuk GaN, InGaN dan InAlGaN telah digunakan dalam kajian ini. Kajian ini telah dimulakan dengan fabrikasi GaN berliang. Analisis struktur menunjukkan bahawa liang berbentuk heksagon telah diperolehi dengan peningkatan permukaan kekasaran relatif kepada sampel tidak berliang. Berikutan itu, fabrikasi InGaN berliang telah dijalankan. Kesan masa punaran mendedahkan bahawa saiz dan ketumpatan liang meningkat dengan masa punaran. Aktiviti punaran di sempadan menjadi lebih signifikan untuk tempoh punaran yang lebih lama di mana kawasan yang tidak sempurna di sempadan telah dipunarkan. Pengurangan ketumpatan kehelan disebabkan oleh proses punaran dan telah disahkan oleh nilai yang menurun pada FWHM dari HR-XRD rocking curve untuk semua sampel InGaN berliang. Keamatan fotoluminesen (PL) bagi sampel InGaN berliang meningkat secara beransur-ansur dengan masa punaran dan PL spektrum menunjukkan anjakan merah berbanding InGaN tidak berliang yang menunjukkan peningkatan dalam sifat optik dan saintaian tegasan telah berlaku dalam

sampel berliang. Selain daripada itu, fabrikasi sampel kuaternari berliang juga telah dibina pada substrat yang berbeza dan dibandingkan. Sampel InAlGa_N/nilam berliang mempamerkan bentuk liang bulat manakala InAlGa_N/Si(111) berliang menunjukkan seperti struktur berliang karang. Semua sampel berliang menunjukkan peningkatan dalam kepadatan dan saiz liang dengan masa punaran dan pameran luas permukaan yang tinggi berbanding sampel tidak berliang. Puncak E₂ (high) bagi sampel berliang mengalami anjakan berbanding dengan sampel bukan berliang dalam spektrum Raman dan ini menunjukkan kelonggaran tekanan dalam sampel berliang. Seterusnya, GaN, InGa_N dan InAlGa_N berliang telah digunakan bagi aplikasi untuk penderia gas hidrogen. Penderia gas hidrogen berasaskan sample tidak berliang dan berliang telah difabrikasikan dan dibandingkan. Perubahan SBH, ($\Delta\phi_B$) apabila terdedah kepada 0.1% H₂ dalam gas N₂ meningkat secara beransur-ansur dengan masa punaran dan mencapai nilai maksimum pada 10 minit punaran dengan faktor 3.2 berbanding dengan sample tidak berliang. Penderia gas hidrogen berasaskan sampel berliang menunjukkan perubahan arus yang ketara semasa dialirkan gas hidrogen dan mempamerkan kepekaan yang lebih tinggi berbanding dengan penderia gas hidrogen berasaskan sampel tidak berliang. Kepekaan penderiaan gas hidrogen InAlGa_N yang optimum (punaran selama 10 minit) adalah kira-kira 6.9 lebih tinggi daripada penderia gas InAlGa_N tidak berliang, dengan masa tindak balas dan pemulihan sebanyak 13.8 saat dan 88.4 saat, masing-masing, pada suhu bilik. Tambahan pula, tindak balas arus meningkat secara beransur-ansur dengan kadar aliran hidrogen bagi sampel ini. Kajian ini menunjukkan bahawa struktur berliang mempunyai pengaruh yang besar ke arah sifat-sifat semikonduktor III-nitrida. Kajian ini juga menunjukkan penghasilan struktur berliang yang bagus pada permukaan filem III-nitrida dengan menggunakan teknik yang mudah iaitu teknik punaran PEC untuk peranti penderiaan gas hidrogen.

**FABRICATION AND CHARACTERIZATION OF POROUS III-
NITRIDES ALLOYS FOR APPLICATION IN HYDROGEN GAS SENSING
DEVICES**

ABSTRACT

The main goal of this work was to fabricate porous III-nitrides structures and utilize them in hydrogen gas sensing devices. The pores were formed on the III-nitrides films to reduce the dislocation density in III-nitrides layer and produce high surface area to volume ratio for high performance gas sensor application. The photoelectrochemical (PEC) etching technique was used to fabricate porous GaN, InGaN and InAlGaN which refer to binary, ternary and quaternary compounds of III-nitrides, respectively. N-type GaN, InGaN and unintentionally doped n-type InAlGaN samples were used in this study. The study began with the fabrication of porous GaN. Structural analysis revealed a hexagonal pore shape and increased surface roughness relative to the non-porous sample. Next, porous InGaN was fabricated. The effect of etching duration revealed that the pore size and density increased with etching duration. The etching activity at the grain boundaries became significant for longer etching duration in which more defective regions at grain boundaries had been etched. The reduction in dislocation density due to the etching process was confirmed by a decreased value of the full width at half maximum (FWHM) from high resolution x-ray diffraction (HR-XRD) rocking curve measurements for all porous InGaN samples. The photoluminescence (PL) intensity of porous InGaN samples increased gradually with etching duration and the PL spectra showed a slight red shift compared to non-porous InGaN; these results indicate that optical properties have been enhanced and stress relaxation has taken place in the porous samples, respectively. Finally, porous

quaternary samples were fabricated on different substrates and compared. The porous InAlGaN/sapphire sample exhibited a circular pore shape, whereas the pore shape of porous InAlGaN/Si(111) was coral-like porous structure. All porous samples exhibited increased pore density and size with etching duration and had a high surface area to volume ratio compared to the non-porous sample. The E_2 (high) peak of porous samples was observed to be shifted relative to non-porous sample in Raman spectra suggesting relaxation of stress in the porous samples. In the next part of the study, porous (GaN, InGaN and InAlGaN) based and non-porous based hydrogen gas sensors were fabricated and compared. The change in Schottky barrier heights (SBH) ($\Delta\phi_B$) upon exposure to 0.1% H_2 in N_2 gas increased gradually with etching duration and reached the maximum value at 10 minutes of etching by a factor of about 3.2 relative to that of the non-porous sample. Porous based hydrogen gas sensors showed a significant change of current upon introduction of hydrogen gas and exhibited higher sensitivity compared to the non-porous based hydrogen gas sensor. The sensing response of the optimum InAlGaN-based hydrogen gas sensor (etched for 10 min) was about 6.9 higher than that of the non-porous InAlGaN gas sensor, with response and recovery times of 13.8 seconds and 88.4 seconds, respectively, at room temperature. Furthermore, the current response increased gradually with hydrogen flow rate for this sample. The results of this study illustrate the feasibility of producing good porous structure on III-nitrides films via PEC etching for potential use in hydrogen gas sensing devices.

CHAPTER 1

INTRODUCTION

1.1 Introduction to III-Nitrides

III-nitrides semiconductors, which include AlN, GaN and InN and their related alloys, have been widely studied as potential materials for use in optoelectronics and electronics applications due to their superior properties such as direct and wide bandgap. The band gap values of InN, GaN and AlN are reported to be 0.7, 3.4 and 6.2 eV, respectively (Wu and Walukiewicz, 2003). The wide range of direct bandgaps makes III-nitrides attractive for optoelectronics applications such as light emitting diodes (LEDs) (Han et al., 2014; Li et al., 2016), photodetectors (Bao et al., 2013; Zhang et al., 2016) and laser diodes (Alahyarizadeh and Rahmani, 2016; Cai et al., 2016). Generally, III-nitrides semiconductors can be crystallized into both wurtzite and zinc-blende polytypes. However, the former is more widely studied because it is more thermodynamically stable.

III-nitrides semiconductors have also been utilized for high temperature/high-frequency applications. For example, the wide band gap nature of GaN allows the material to go intrinsic at much higher temperature. Other attractive properties of III-nitrides include high breakdown fields, excellent electron transport properties, high saturated drift velocity, and high mechanical and thermal stability (Pearson et al., 2000).

Ternary and quaternary III-nitrides have been further studied in recent years due to their potential to overcome the shortfalls of binary III-nitrides (Li et al., 2001). $\text{In}_x\text{Ga}_{1-x}\text{N}$ ternary and $\text{In}_x\text{Al}_y\text{Ga}_{1-x-y}\text{N}$ quaternary alloys are currently major topics of research. The direct bandgap can be tuned from 0.7 to 6.2 eV, which spans the range

from infra-red (IR) to deep ultra-violet (UV) regions. This tuning can be accomplished by varying the In and Al compositions in the material system. This feature makes the III-nitrides alloys attractive for use in optoelectronics and sensing devices such as LEDs and photodetectors (Oder et al., 2000; Nagarajan et al., 2008; Han et al., 2014; Huang et al., 2014).

1.2 Research Problem and Motivation

III-nitrides semiconductors represent a promising material for use in optoelectronic and sensing devices (Schalwig et al., 2002a; Ali et al., 2006; Chang et al., 2010). Fabricating a highly efficient and reliable device requires a high quality crystalline layer of the III-nitrides. However, growing a high quality III-nitrides layer is not an easy task due to the lack of suitable substrate. III-nitrides semiconductor such as GaN is commonly grown on sapphire or Si (111) substrate, but they have a high lattice mismatch of 13.6% and 17%, respectively (Pearson, 1997). In addition, sapphire exhibits a higher thermal expansion coefficient with $a=7.5 \times 10^{-6} \text{ K}^{-1}$, $c=8.5 \times 10^{-6} \text{ K}^{-1}$ to GaN with $a=5.59 \times 10^{-6} \text{ K}^{-1}$ and $c=3.17 \times 10^{-6} \text{ K}^{-1}$. For Si (111), the thermal expansion coefficient is smaller with $a=c=3.59 \times 10^{-6} \text{ K}^{-1}$ than GaN (Popovici and Morkoc, 2000). This high level of lattice mismatch and thermal expansion coefficient difference between the epilayer and the substrate will result in high defects and dislocation density, and it will increase the strain in the III-nitrides layer during the epitaxial growth (Vajpeyi et al., 2005a), which in turn will degrade the epitaxial quality. Although 6H-SiC has the lowest lattice mismatch of 3.5% with GaN (Pearson, 1997), it is expensive and thus unsuitable for commercial purpose. Such problems would considerably limit the efficiency of the devices. Therefore,

improving the quality of III-nitrides layer is of crucial task to obtain high reliability devices.

Several approaches have been applied to overcome these problems. For example, researchers have tried growing GaN layer on low-temperature AlN buffer layer (Zhang et al., 2004a; Zhang et al., 2004b) or using other materials, such as scandium nitrite, as interlayer (Moram et al., 2007). Modifying the III-nitrides structure also has become an alternative strategy for providing better nitride epitaxy.

Therefore, there are several reasons for fabricating porous structure on III-nitrides layer. This is because porous structure could offer several advantages compared to conventional bulk materials (Huang et al., 2013; Cheah et al., 2015). Porous structure can reduce the defect density and relieve strain caused by lattice mismatch (Lin et al., 2006). Moreover, a porous GaN template could reduce the dislocation density and allow high quality GaN overgrowth (Hartono et al., 2007b). Porous GaN has exhibited more efficient luminescence relative to non-porous GaN (Vajpeyi et al., 2005b) and the porous structures produce the high surface area to volume ratio needed for optoelectronics and gas sensor applications (Duan and Bohn, 2010; Zhang et al., 2016).

Thus, understanding the properties of porous III-nitrides, which could improve the structural and optical properties of III-nitrides materials and identifying their potential applications in sensing device are the motivation for this research. From the literature, previous works on porous III-nitrides have focused mainly on the fabrication of porous GaN (binary compound). Very little research exists on the porous InGaN (ternary compound) and to our best knowledge, the fabrication of porous InAlGaN (quaternary compound) has not been reported so far. Therefore, in this work, the study of porous III-nitrides began with porous GaN and the ability to

fabricate porous GaN effectively using PEC etching method has driven a motivation to apply such technique in producing porous InGaN and porous InAlGaN. Moreover, the study of porous InGaN and InAlGaN is still at the early stage, and most of their fundamental properties are not yet well established and not available in the literature. Thus, this motivates our work to explore the properties of this new form of material and its potential application. Although porous InGaN and InAlGaN already have been applied in the development of LEDs and photodetectors (Han et al., 2014; Yu-Hsuan et al., 2013; Zhang et al., 2013), their use in hydrogen gas sensors has not been reported previously in the literature. On top of that, the excellent properties of InGaN and InAlGaN make ternary and quaternary porous III-nitrides versatile for designing advanced gas sensor devices. Furthermore, it should be possible to integrate porous InGaN or InAlGaN gas sensors into InGaN- or InAlGaN-based optoelectronics devices on the same chip.

1.3 Research Objectives

The main focus of this project was the investigation of the porous structure of III-nitrides semiconductors, covering the binary, ternary and quaternary compounds of nitrides materials (GaN, InGaN and InAlGaN). The porous structure was generated using photoelectrochemical etching (PEC) technique. In order to access to better fundamental understanding of the properties of the III-nitrides semiconductor, the project began with investigation of the morphological, structural and optical characteristics of the non-porous III-nitrides. Next, porous GaN was fabricated and its properties were characterized with the same tools used to study the non-porous materials. Subsequently, porous InGaN and InAlGaN were fabricated; the structure and properties of these materials have not been reported previously in the literature.

The characterization measurements for all samples helped to determine the possibilities of the best porous samples to be used for hydrogen gas sensor applications. Ultimately, porous GaN- InGaN- and InAlGaN-based hydrogen gas sensors were fabricated and compared to the non-porous gas sensor. The best device was identified based on sensitivity, response and recovery times.

The objectives of this work were as follows:-

1. To investigate the morphological, structural and optical characteristics of non-porous and porous GaN.
2. To study the morphological, structural and optical properties of porous InGaN (ternary compound) and InAlGaN (quaternary compound).
3. To compare the characteristic and performance of non-porous and porous GaN, InGaN and InAlGaN hydrogen gas sensor based on sensitivity, response and recovery times.

1.4 Originality of the Research Work

The originality of this research work includes the following key points:-

1. Despite excellent progress in understanding porous III-nitrides compounds, research activities remain largely focused on binary compounds, particularly GaN. To date, very little research has focused on the porous ternary InGaN, and various parameters of the etching process have not yet been explored. To the best of our knowledge, fabrication of porous InGaN using potassium hydroxide (KOH) solution with different etching durations and the effect of using different light

sources on the properties of porous InGaN have not yet been reported in the literature.

2. Fabrication and investigation of the porous structure of other types of III-nitrides materials such as quaternary InAlGaN is presented here for the first time.
3. This study includes efforts to enhance the properties of InGaN and InAlGaN by the formation of the porous structure on the thin films.
4. The fabrication and investigation of hydrogen gas sensors based on porous InGaN and InAlGaN is described here for the first time.

1.5 Limitation of Study

Although the research has reached its objective, there was unavoidable limitation. The availability of the samples was limited especially for GaN and InGaN samples. Therefore, due to the limitation of the samples, the research was handled carefully in order not to waste the samples. For the fabrication of porous GaN and InGaN structure under different etching duration, the parameter was conducted and planned wisely in order to obtain sufficient data.

1.6 Outline of the Thesis

This thesis consists of eight chapters describing work on the porous III-nitrides (porous GaN, InGaN and InAlGaN) fabricated using the PEC etching technique and the application of these porous materials in hydrogen gas sensors. This thesis is organized as follows:

Chapter 1 presents an overview of III-nitrides as well as the research problems, motivation and objectives of the work.

In Chapter 2, a survey on the published data regarding porous III-nitrides is presented, and issues and techniques used to fabricate the porous structure are described. In addition, the potential of the porous structure to be adopted for application in hydrogen sensing device is described.

Chapter 3 presents the general principles and theories of PEC etching of porous III-nitrides, metal-semiconductor contact and hydrogen gas sensor.

Chapter 4 describes the methodology and instrumentation used in this study.

The results obtained from the research works are analyzed and discussed in Chapter 5 (porous GaN), 6 (porous InGaN) and 7 (porous InAlGaN). The performance of the hydrogen gas sensor devices fabricated based on each porous material are described at the end of each chapter.

Finally, Chapter 8 summarizes the findings of this research work. Suggestions for the future work are also included in this chapter.

CHAPTER 2

LITERATURE REVIEW

2.1 Introduction

The applicability of III-nitrides semiconductors has been studied for many optoelectronics and sensing devices. However, several issues such as high dislocation density due to large lattice and thermal mismatch between the III-nitrides epilayer and the substrate, can hinder the performance of the device. Therefore, studies of how to improve the properties of porous III-nitrides using PEC and electroless etching techniques are needed. Until now, studies of porous III-nitrides have been focused mainly on porous GaN which is a binary compound. Limited data are available for porous InGaN (ternary compound), and to our knowledge, no information about porous InAlGaN (quaternary compound) and its application in sensing devices has been published. This chapter provides a brief overview of porous semiconductors and the development of porous III-nitrides, including porous GaN and InGaN. The application of porous III-nitrides in hydrogen gas sensors is also described. Figure 2.1 provides an overview of the literature search and the existing research gaps.

2.2 Overview of Porous Semiconductors

Nano-structure materials have drawn a great deal of attention due to their unique chemical and physical properties, which include small size and vast surface to volume ratio. In addition, such materials have become promising material and being explored for the application in many semiconductor devices. Therefore, a comprehensive study of porous semiconductors is needed.

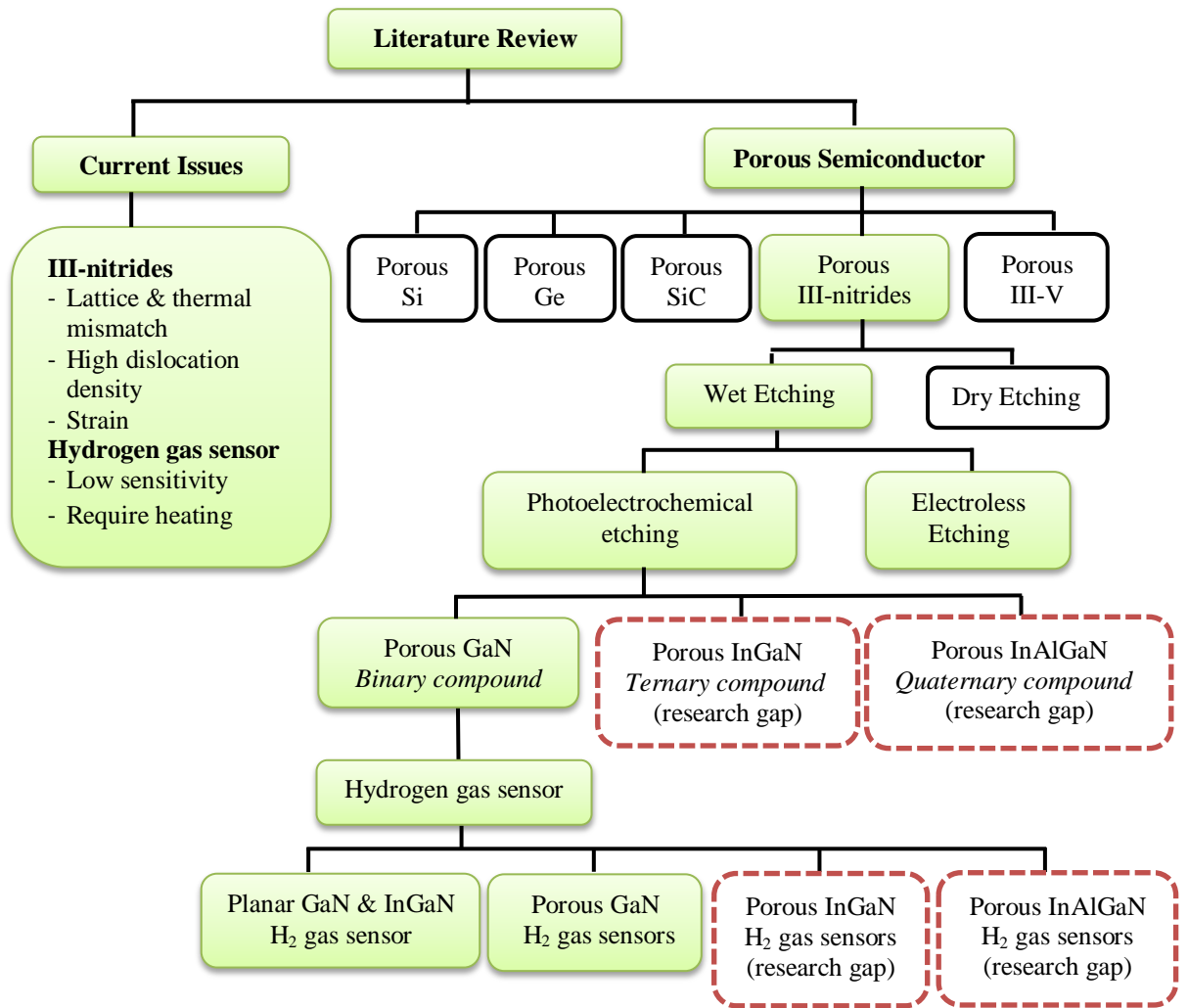


Figure 2.1: Schematic diagram of literature review and existing research gaps

Porous semiconductor is the semiconducting material with open pores which increase the surface area to volume ratio on the surface of the material that can be fabricated via etching processes. Studies of porous semiconductors have increased steadily over the recent decades due to their superior properties over their bulk counterparts. The porous semiconductor can act as a sink for mismatch dislocation and accommodate the strain in epilayers (Ponce and Bour, 1997; Díaz et al., 2002). Porous semiconductors also offer improved optical properties, such as shifting of the emission wavelength and enhancement of luminescence efficiency, compared to their

non-porous semiconductors (Canham, 1990; Naderi and Hashim, 2012). Moreover, the high surface to volume ratio of porous semiconductors is good for use in sensing application devices (Dubey and Gautam, 2011; Rani et al., 2013; Siciliano et al., 2014; Zhang et al., 2016).

The first porous semiconductor was initially started with porous silicon that was accidentally encountered by Uhlir at Bell Laboratories in 1956 (Uhlir, 1956). During an electropolishing experiment of a Si wafer, he discovered that fine holes were produced on the surface of Si instead of dissolving the Si uniformly. Later, Canham (1990) observed intense visible photoluminescence (PL) emission from porous silicon. This observation triggered further investigations, and significant advancements have been made in understanding the optical and structural properties of porous semiconductor materials (Dubin, 1992; Cullis et al., 1997; Li and Bohn, 2000; Nahor et al., 2014). Among porous semiconductors, porous Si has been rigorously studied due to its low-cost. However, porous Si is unstable in terms of its chemical, thermal, and mechanical properties as well as it has weak electroluminescence efficiency. This has led to the development of other porous semiconductors.

Apart from Si, other semiconductors such as SiC, Ge, III-V compounds (GaAs, GaP and InP) and III-nitrides are receiving more interest in the porous semiconductor activity. For example, porous SiC which has an indirect bandgap, was first explored by Shor et al. (1993) and it is the most studied compound after porous Si. This material has been used to develop shorter wavelength emitting devices (Mimura et al., 1994), gas sensors (Kim and Chung, 2011; Keffous et al., 2013) and photodiodes (Boukezzata et al., 2008; Keffous et al., 2010).

Ge is another type of porous semiconductor that has been studied extensively. Ge is an indirect semiconductor that is useful for near infrared photodiodes and x-ray detector applications. The fabrication of porous Ge was first discovered by Beckmann (1966) by using stain etching technique in a diluted solution of HF/H₂O₂. Subsequently, the study of porous Ge was reported by other research groups (Bayliss et al., 1996; Chang and Hummel, 2000; Guzmán et al., 2008; Romano et al., 2013). Although many optoelectronics devices are being developed using these indirect semiconductor materials, the efficiency of the devices does not compare favorably with that of devices containing direct semiconductor materials such as III-V compounds and III-nitrides.

Research activities further continued to explore the properties of porous III-V compounds. For example, InP has direct bandgap and is widely used for high-speed electronics and optoelectronic devices. Porous InP was first discovered via an electrochemical anodization technique (Toshiyuki et al., 1994). Later, Hamamatsu et al. (1999) successfully produced highly ordered porous nanostructures using PEC anodization method with illumination from a tungsten lamp. In both studies, the anodization was conducted in HCl electrolyte. Then, there were other subsequent studies on porous InP (Tsuchiya et al., 2004; Seo and Yamaya, 2005; Leisner et al., 2010; Kumazaki et al., 2013) and the material was used for application in solar cells (Sato et al., 2010) and gas sensors (Volciuc et al., 2010). GaAs is another III-V compound that has direct bandgap and high carrier mobility which is extensively used in Schottky diodes, LEDs, and laser. Krumme and Straumanis (1967) first fabricated porous GaAs by anodic etching. Later, porous GaAs fabricated in aqueous KOH were observed to have large pores (Faktor et al., 1975), whereas anodization of GaAs in HF was found to promote high density of pores. One downside of porous

GaAs is that the amount of gallium composition was reported to decrease during the etching process (Beale et al., 1985; Ali et al., 2009). Moreover, anodization of GaAs tends to produce oxide (arsenic oxide) in the porous layer, which is undesirable for high quality epitaxial growth (Lockwood et al., 1999; Mazouz et al., 2011).

2.3 Overview of Porous III-nitrides

III-nitrides based materials have become the candidate of choice for use in photonics and sensing applications in recent years due to their unique and excellent properties. The wide direct bandgap and robust properties of III-nitrides materials such as GaN make it attractive for use in high temperature applications and also in harsh environments. III-nitrides related alloys such as ternary InGaN and quaternary InAlGaN further boost the properties of III-nitrides materials. The direct bandgap of these alloys can be varied from IR to UV regions by varying the In and Al composition in the alloy system, which allows greater flexibility and versatility in designing devices. Moreover, generating porous structure on the III-nitrides thin films is expected to improve the film structural and optical properties such as reduction of defect density and increment of luminescence signal (Hartono et al., 2007a; Cheah et al., 2015). Such properties are good for the better performance of application devices. An overview of III-nitrides semiconductors and their related alloys can be found in section 1.1

Interest in porous III-nitrides has grown due to their superior properties over non-porous film. The porous structure has the ability to reduce the dislocation density and relief the strain that originated from the lattice mismatch between the III-nitrides layer and the native substrate (Lin et al., 2006; Soh et al., 2013). The improved properties of porous III-nitrides layer are due to the removal of the

defective region at the grain boundaries by KOH solution during the etching process (Cho et al., 1999; Zhao et al., 2006). Therefore, the porous structure could improve the properties of III-nitrides films, which is important for the fabrication of high performance and reliable devices.

Furthermore, porous III-nitrides structure provides stress relaxation compared to the non-porous structure. Thus, porous III-nitrides are attractive options for use as a growth template for the subsequent III-nitrides layer growth (Inoki et al., 2003; Hartono et al., 2007a; Soh et al., 2009; Jang et al., 2014). In fact, porous III-nitrides as the growth template probably is the best solution for growing high quality III-nitrides layer because of having the same lattice and thermal expansion coefficient. Thus, the large dislocation density and strain in the epitaxial layer would be reduced. Hartono et. al (2007a) reported that growing GaN on a strain-relaxed porous GaN template led to a reduction in threading dislocation density of up to 60% and the porous GaN structure could minimize the propagation of threading dislocation into the subsequently overgrown GaN film (Soh et al., 2009; Soh et al., 2013).

In addition to the reduction of dislocation density and strain management in epitaxial layer, porous III-nitrides structure also has a high surface area to volume ratio, which is useful for sensing applications such as gas sensors. Several research groups have reported the application of porous GaN for gas sensor devices (Yam et al., 2007b; Yam and Hassan, 2007; Al-Heuseen and Hashim, 2012; Zhong et al., 2014a; Zhong et al., 2014b). The porous GaN gas sensors showed enhanced sensing performance compared to the non-porous GaN gas sensor due to the increase of sensing area in the porous GaN structure.

Apart from the interesting structural properties of porous III-nitrides, porous GaN exhibits improved optical properties, such as a shift in the emission wavelength

and enhanced luminescence efficiency, relative to the non-porous GaN (Vajpeyi et al., 2005a; Hartono et al., 2007b; Cheah et al., 2015). Such characteristics are beneficial for optical device applications.

Therefore, in order to realize the potential of porous III-nitrides in various applications, the issue to determine the precise control of porous III-nitrides properties such as the pore density and size is essential. These properties affect device performance. Hence, the challenge in fabricating porous III-nitrides lies on how to control the etching parameters during the etching process to generate the desired porous morphologies.

2.4 Overview of the Process of Fabricating Porous III-nitrides

Porous III-nitrides can be considered relatively less studied compared to other semiconductor materials such as Si and III-V semiconductor. Research on porous III-nitrides began with the binary compound, which is porous GaN, that was fabricated by Mynbaeva and Tsvetkov (1997). Since the achievement in fabricating the first porous GaN, this group actively continues the research on porous GaN (Mynbaeva et al., 2000; Mynbaeva et al., 2011). Later, many other researchers also have shown interest in porous GaN (Diaz et al., 2003; Chen et al., 2012; Huang et al., 2013) . Apart from the tremendous research of porous GaN, few studies of the porous III-nitrides ternary compound, which is porous InGaN have been published (Saleh et al., 2012; Ramizy et al., 2015). However, the research in porous InGaN is at the early stage and many basic fundamental properties have not yet been identified. In the following sections, the fabrication of both porous GaN and InGaN will be described.

2.4.1 Fabrication of Porous III-nitrides by Bottom-up Technique

Porous III-nitrides such as porous GaN and InGaN can be produced using several techniques. For example, several research groups generated porous GaN using bottom-up technique in which the porous structure generated during the growth process of the thin film using chemical vapor deposition (CVD) or ion-beam assisted molecular beam epitaxy (MBE) system. Caravajal et al. (2008) produced GaN nanoporous particles by the direct reaction of Ga and NH₃ in a CVD system. They reported the influence of different parameters, such as temperature, flow rate of ammonia and pressure on the porous GaN morphology. However, the structural and optical properties of the GaN nanoporous particles were not characterized to support the potential of porous GaN for device applications. Bilousov et al. (2014) described a similar technique for producing porous GaN particles. Nevertheless, the porous structure obtained was not dense and they did not provide a clear image of the porous structure. Poppitz et al. (2014) produced dense porous GaN nanowall networks using MBE. Nevertheless, the x-ray diffraction rocking curve showed that the crystalline quality of the obtained porous film was of lower quality relative to that of a typical epitaxial GaN thin film (Neumann et al., 2012). Moreover, the fabrication of porous GaN structure by bottom-up technique or growth processes such as CVD and MBE is complicated and expensive process.

2.4.2 Fabrication of Porous III-nitrides by Dry Etching Technique

Porous III-nitrides can be fabricated using etching techniques (top-down), which can be classified as either dry or wet etching. Generally, dry etching technique which include reactive ion etching, inductively coupled plasma reactive ion etching and chemical assisted ion beam etching have been used to fabricate many porous

structures (Kucheyev et al., 2000; Cheung et al., 2011; Hajj-Hassan et al., 2011). Nevertheless, the challenge of this technique lies in the plasma-induced damage to the surface of the film which subsequently degrades the quality of the material and device performance (Choi et al., 2000; Choi et al., 2002; Wang et al., 2014b). In other work reported by Wang et al. (2005), the fabrication of porous GaN by inductively coupled plasma etching using aluminum oxide film as an etch mask generated ordered porous arrays on GaN thin film. However, this approach is quite complicated because it involves a two-step anodization process of the aluminum film prior to the inductively coupled plasma (ICP) etching. On top of that, the dry etching technique also requires a high vacuum environment and plasma generation, which is costly.

2.4.3 Fabrication of Porous III-nitrides by Wet Etching Technique

Wet etching technique offers more reliable and convenient method for the fabrication of porous III-nitrides because this technique requires only simple and inexpensive equipment compared to the dry etching technique. From the literature, two wet etching techniques are commonly used to generate porous III-nitrides: (i) metal-assisted electroless etching and (ii) PEC etching.

2.4.3(a) Metal-assisted Electroless Etching

The metal-assisted electroless etching technique requires no electrical contact to the sample. This technique involves deposition of a thin layer of metal islands on the sample surface followed by the electroless etching process, which takes place in aqueous solution under UV illumination. A strong oxidizing agent is added to the

aqueous solution to oxidize the semiconductor surface. Several research groups have investigated this etching technique for the fabrication of porous GaN.

Electroless etching of GaN was developed by Bardwell et al. (2001). They used a solution containing oxidizing agent of peroxydisulfate ($K_2S_2O_8$) and KOH under UV illumination as well as two types of metal masks, Pt and SiO_2 in the etching process. They discovered that Pt as the catalytic mask yielded a higher etch rate compared to SiO_2 . However, a non-uniform morphology of the porous structure was observed due to different etch rates that depended on the distance from the Pt mask. In addition, the low defect density regions were preferentially etched over the grain boundaries and dislocation regions. Thus, the crystalline material was removed during the electroless etching process and the dislocation region remained which was visible as needle-like dislocations (Bardwell et al., 2001). In relation to that, an additional and careful sonication step was required to remove the dislocations without disturbing the underlying porous structure.

The research works on electroless etching of GaN was further investigated intensively by P. W. Bohn's research group (Díaz et al., 2002; Diaz et al., 2003; Guo et al., 2006; Li et al., 2002; Geng et al., 2013) and Yam et al. (Yam and Hassan, 2009; Yam et al., 2007a). The GaN film was etched in a solution of $CH_3OH:HF:H_2O_2$. The morphology of the etched sample showed the formation of ridge structures, with a deep porous network between and under the ridges. Similar to the report by Bardwell et. al. (2001), the electroless etching of GaN presented by P. W. Bohn group also resulted in removal of the crystalline material and leaving the dislocation region. The presence of ridges composed of dislocations can be seen on the surface of porous GaN and they need to be removed by sonication process. However, some of the highly branched layers at the surface of porous GaN were

removed during the sonication process, which resulted in larger pores in the porous structure (Williamson, 2000). This shows that the initial porous structure was disturbed by the sonication process.

Moreover, among the metal used for electroless etching, the Pt island film has been confirmed as an effective catalyst and it yielded rapid etching of GaN (Yam and Hassan, 2009; Duan and Bohn, 2010; Geng et al., 2013). Nevertheless, the issue of this technique lies in the difficulty of removing the Pt after metal-assisted electroless etching without destroying the porous GaN structure because of the insoluble properties of Pt. The residual metal somehow affects the performance of devices that utilize porous GaN structure (Geng et al., 2013). Besides that, this approach also lacks the ability to control the pore size and distribution of pores across the whole sample. The morphology of the porous structure may vary with position relative to the deposited metal film (Geng et al., 2013), with the region adjacent to the metal film showing a higher density of pores compared to regions further away from the metal film. In relation to that, a comparative study of the fabrication of porous GaN using metal-assisted electroless etching and PEC etching technique has been reported by Vajpeyi et al. (2005b). They have confirmed that PEC etching technique produced more uniform pore size of the porous GaN structure than that been obtained by electroless etching technique.

2.4.3(b) Photoelectrochemical (PEC) Etching

Another common technique for the fabrication of porous III-nitride is PEC etching. PEC etching technique involves the use of electrolytes, an external potential and a UV light source. UV illumination is used for photo-generation of electron-hole pairs to facilitate the etching process. This technique is suitable for fabricating porous III-nitrides due to its low surface damage of the thin film, versatility and

capable of controlling the pore size and etching depth by varying the etching conditions. The etching parameters which include the type and concentration of the electrolyte, etching voltage, etching duration and type of light source will affect the structural and optical properties of the porous structure. Careful control of these parameters during the etching process plays a significant role in generating the required porous structure.

Several studies have reported the fabrication of porous III-nitrides using PEC etching techniques. Mynbaeva and Tsvetkov (1997) were the first to explore the fabrication of porous GaN (with SiC as the substrate) using this technique. In their study, the porous GaN sample showed a uniform porous structure with the maximum size of the pore in micrometer scale. X-ray analysis revealed that the fabricated porous GaN had a monocrystalline structure and the rocking curve (RC) for the porous GaN sample was narrower than that of the non-porous GaN. In addition, although luminescence signal was detected from the porous GaN sample, however, no enhancement of the luminescence signal was observed. Another work of porous GaN did by Mynbaeva et al. (2000) using the same technique discovered that the pores were propagated along the dislocation boundaries and subsequently the defect areas were removed during PEC etching of the GaN film. They also found that the formation of pores reduced the residual stress in the porous GaN layer relative to the non-porous GaN.

Studies of fabrication of porous GaN (with sapphire as the substrate) using the PEC etching technique were continued by Vajpeyi et al. (2005a; 2005b; 2007). The porous GaN samples were fabricated using HF solution the electrolyte. The shape of the pores was nearly spheroid with an average pore size of <100 nm, which is much smaller than that of the porous GaN obtained by Mynbaeva and Tsvetkov (1997).

Vajpeyi et al. observed a red-shift of band edge photoluminescence (PL) peak and E_2 phonon peak in Raman spectra from porous GaN compared to non-porous GaN sample. The red-shifted peak indicates that relaxation of compressive stress occurred in the porous GaN. In addition, they reported that smaller pore size resulted in significant stress relaxation (Vajpeyi et al., 2005a; Vajpeyi et al., 2005b; Vajpeyi et al., 2007). Thus, porous GaN become attractive to be used as a growth template for the III-nitrides layer, as discussed in section 2.2. Moreover, in contrast to the report by Mynbaeva and Tsvetkov (1997), the porous GaN exhibited enhanced PL intensity at ~ 357 nm compared to the non-porous GaN, in which the smallest size nanopores showed the highest PL intensity. In other studies, Hartono et al. (2007b; 2007a) observed the amplification of PL intensity in their porous GaN that was fabricated using the PEC etching technique. The amplification of PL intensity is related to the reduction of the defects density and strain in the porous GaN sample, which has a positive effect on the luminescence efficiency of the film. The lower value of the rocking curve (RC) measurement from XRD for porous GaN compared to the non-porous GaN sample showed a reduction in dislocation density in porous samples. Moreover, the light scattering in the pores and the scattering off the crystallite side walls also contribute towards the enhancement of the luminescence efficiency (Vajpeyi et al., 2006; Hartono et al., 2007b; Al-Heuseen et al., 2011a).

On the other hand, Yam et al. (2007c) performed PEC etching on unintentionally doped GaN (with sapphire as the substrate) to examine the effects of different KOH electrolyte concentrations, anodization times and applied voltages on the morphologies of porous GaN. The scanning electron microscopy (SEM) image revealed that the pore size of the porous samples varied widely and the pores has various shapes, including spherical, elongated and triangular. The porous GaN